Nanoscale

RSC Publishing

PAPER

View Article Online
View Journal | View Issue

Cite this: *Nanoscale*, 2013, **5**, 11079

Comprehensive characterizations of nanoparticle biodistribution following systemic injection in mice†

Wei-Yin Liao,‡[a] Hui-Jing Li,‡[a] Ming-Yao Chang,‡[b] Alan C. L. Tang,[a] Allan S. Hoffman[c] and Patrick C. H. Hsieh*[abcd]

Received 30th July 2013
Accepted 3rd September 2013

DOI: 10.1039/c3nr03954d

www.rsc.org/nanoscale

Various nanoparticle (NP) properties such as shape and surface charge have been studied in an attempt to enhance the efficacy of NPs in biomedical applications. When trying to undermine the precise biodistribution of NPs within the target organs, the analytical method becomes the determining factor in measuring the precise quantity of distributed NPs. High performance liquid chromatography (HPLC) represents a more powerful tool in quantifying NP biodistribution compared to conventional analytical methods such as an *in vivo* imaging system (IVIS). This, in part, is due to better curve linearity offered by HPLC than IVIS. Furthermore, HPLC enables us to fully analyze each gram of NPs present in the organs without compromising the signals and the depth-related sensitivity as is the case in IVIS measurements. In addition, we found that changing physiological conditions improved large NP (200–500 nm) distribution in brain tissue. These results reveal the importance of selecting analytic tools and physiological environment when characterizing NP biodistribution for future nanoscale toxicology, therapeutics and diagnostics.

Introduction

Nanoparticles (NPs), an intersection of nanotechnology and biomaterials,[1,2] have been widely used in the biomedical field over the past decade in areas such as drug delivery,[3,4] tissue engineering,[5,6] and molecular imaging.[7,8] In order to further the development of analytic techniques and materials, it is important to first develop an understanding of the effects of NP properties in medicine, including size, shape, surface charge, and functional groups. These physical and chemical properties have been reported to influence the cellular uptake, toxicity, biodistribution, retention, and excretion of NPs.[9–11] Thus, to improve NP therapies, we must first acquire a deeper understanding of the contribution of NPs to biological outcomes.

The closeness of size between NPs and biological molecules is a property often being taken advantage of when designing cell targeting.[12,13] As prior studies have demonstrated that particle size greatly affects its transport mechanisms and fates, scientists now manipulate the size of NPs in an attempt to achieve enhanced, targeted drug delivery.[14,15] One such technique, high performance liquid chromatography (HPLC), takes advantage of the chromatography used in analytic chemistry and biochemistry for substance separation, purification, and quantification. Equipped with fluorescence and UV/VIS detectors, HPLC is able to analyze various molecules including NPs.[16] However, despite possessing the ability to analyze NPs, a comprehensive and systematic evaluation of the effects of NP size on their biodistribution has yet to be established.

Previous studies on NP biodistribution mainly focused on analytic methods specific to particular NPs and occasionally contained sensitivity issues.[17] Here, we use three independent assays to characterize the effects of different NP sizes following systemic administration, including an *in vivo* imaging system (IVIS), HPLC, and immunohistology. Among these assays, HPLC provides the most accurate measurements when quantifying tiny amounts of NP retained in different organs and tissues. By combining multiple approaches, we aim to establish a biodistribution profile for different NP sizes in the mouse model.

Experimental section

Nanoparticle characterization

The 20, 40, 100, 200, and 500 nm fluorescent carboxylated-polystyrene NP (Invitrogen) solutions were sonicated for 10 minutes and then dispersed in deionized H_2O with 2 mM azide (150 μl stock in 1600 μl H_2O). The surface potential of NPs was determined as their zeta potential (Zetasizer ZS, Malvern Industries).

[a]*Institute of Clinical Medicine, National Cheng Kung University & Hospital, Tainan 704, Taiwan, R.O.C. E-mail: phsieh@mail.ncku.edu.tw; Tel: +886-2-27899170*

[b]*Department of Biomedical Engineering, National Cheng Kung University & Hospital, Tainan 704, Taiwan, R.O.C.*

[c]*Department of Bioengineering, University of Washington, Seattle, WA 98195, USA*

[d]*Institute of Biomedical Sciences, Academia Sinica, Taipei 115, Taiwan, R.O.C.*

† Electronic supplementary information (ESI) available. See DOI: 10.1039/c3nr03954d

‡ W.Y.L., H.J.L. and M.Y.C. contributed equally to the work.

The surface morphology of NPs was examined by transmission electron microscopy (TEM) and scanning electron microscopy (SEM). The NP samples were lyophilized for 24 h and images were taken by an experienced technician using an H-7500 TEM (Hitachi, Japan) and HR FE-SEM (JEOL, JSM-6700F).

Basic/acid resistance and fluorescein equivalent analysis

Three mg of 20, 40, 100, 200, and 500 nm NPs were each incubated in 2 ml of phosphate buffer solution at various pH values, at 37 °C. After 4 hours, the NP solutions were centrifuged and the supernatants were collected for DLS (Malvern Industries) analysis polydispersity index (PDI) and HPLC analysis fluorescence leakage.

Animals and nanoparticle injection

The National Cheng Kung University Animal Care and Use Committee and the National Laboratory Animal Center approved all animal research procedures. FVB and nude mice of either sex (6 to 8 weeks, weight 22 ± 0.6 g) were purchased from the National Laboratory Animal Center.

Fluorescent carboxylated polystyrene latex beads with uniform diameters of 20, 40, 100, 200, and 500 nm (3 mg for each mouse) were used to investigate the biodistribution and retention of NPs after intravenous injection into normal mice. These NPs were non-degradable, thus excluding resorption as a variable. NPs were quantified by HPLC (Jasco FP-2020 plus intelligent Fluorescence Detector, Essex, UK). Fluorescence microscopy and an *in vivo* fluorescence imaging system (IVIS 200, Caliper Life Sciences, Massachusetts, USA) were used to observe the NP biodistribution in the tissues and organs.

To quantify the NP retention, normal, healthy mice were anesthetized with Zoletil (50 mg kg^{-1}; Virbac, France) and Rompun (0.2 ml kg^{-1}; Bayer Healthcare, Germany), and injected with one of the five sizes of NPs or PBS (control group) through the jugular vein (3 mg per mouse). Mice were returned to their cages and received normal diet and water for 4 hours. After 4 hours, the organs and tissues were harvested.

Nanoparticle quantification by HPLC

For HPLC analysis, the harvested tissues, organs and urine were digested in 0.5 or 3 ml of 1 M potassium hydroxide (KOH) solutions at 60 °C overnight, depending on the sample. The brain, heart, lungs, liver, spleen, kidneys, blood, skin and fat were digested in a 0.5 ml volume. Due to the size of the liver, 3 ml of KOH solution was required for complete digestion. All of the samples were then mixed with 0.5 ml of *o*-xylene for dye extraction by sonication for 1 min and placed into a 60 °C oven for 15 minutes. The samples were vortexed and incubated at 60 °C for 5 min; this step was repeated twice. For the urine sample, 0.5 ml of xylene was added directly without KOH digestion. The preparation of these samples then followed the procedures described above. Finally, all of the samples were centrifuged for 30 minutes at 14 000 RPM to separate the dye-containing supernatant and the digested tissues, and then the supernatants were analyzed by HPLC.

Reagents and procedures for HPLC analysis

HPLC-grade methanol (Sigma, USA), which served as the mobile phase and Hypersil™ GOLD C18 columns were used for analysis (Thermo, USA). In the analysis study 20 μl (sample solution) was injected into the HPLC pump (Jasco plus 2080), the mobile phase condition of 100% methanol was used (J.T Baker, 9093-68), with a flow rate of 0.5 ml min^{-1}, for 5 min; and detection was by fluorescence at the excitation and emission of 505 nm and 515 nm, respectively. HPLC standards were measured by sampling 10, 40, 80, 160, and 200 μg of 20, 40, 100, 200, and 500 nm NP solutions. The extraction procedures for NP standards were identical to the protocol described above. The relative amount of NP retention in each sample was calculated using the standard calibration curves.

Immunohistochemistry

Major organs and tissues, including the brain, heart, lungs, liver, spleen, kidneys, skin, fat and blood, and urine, were harvested. For immunohistochemistry imaging, the organs were dehydrated for 6 hours in 15% sucrose solution and then overnight in 30% sucrose solution. After dehydration, the organs were embedded in tissue freezing medium at −20 °C. Immunohistochemistry was subsequently performed with Alexa Fluor® 488 conjugated anti-isolectin antibody (1 : 200, Invitrogen), and nuclei were counterstained with DAPI (1 mg ml^{-1}). Whole field images were acquired using a TissueFAXS system. The magnified image was exported from the region of the original image *via* Tissue Quest analysis system.

Statistical analysis

Results are presented as the mean ± SEM. Statistical comparisons were performed with ANOVA. A probability value of $p < 0.05$ was considered statistically significant. There were at least 6 animals in each group, unless specified.

Results and discussion

Linearity of the calibration curve in HPLC and IVIS

To characterize the size-dependent effects of NPs, commercially available 20, 40, 100, 200, and 500 nm fluorescent polystyrene NPs were acquired. To minimize any variation that affects biological responses of NPs, we used NPs with identical surface modification. All NPs had similar zeta-potentials and uniform size distributions (Table 1). The NPs shapes were confirmed by both TEM and SEM, revealing consistent spherical morphology (Fig. S1†). As a result, we can infer that size is the only variable. Since the bodipy dye trapped within the NPs provides high fluorescence quantum yields and sharp emission peaks, the NPs can be traced *in vitro* or *in vivo* by their fluorescence intensity and photostability.[18,19] To quantify NPs, calibration curves were established in both IVIS and HPLC studies (Fig. 1). For HPLC, the *R*-squared values of the calibration curves were approximately 1, demonstrating a linear trend for the standard samples. In contrast, the *R*-squared values of the IVIS results fell between 0.79 and 0.89. Furthermore, IVIS seemed to be limited in detecting the upper boundary of NP injections when

Table 1 Physical and chemical properties of nanoparticles used in this study

Size	Nanoparticles	Diameter (*z*-average, nm)	Zeta potential[b] (mV)	PDI[a,b]	Count rate[b] (kcps)
20 nm	PS-COOH	24 ± 3.0	−41.86 ± 2.71	0.33 ± 0.04	129.59 ± 22.51
40 nm	PS-COOH	56 ± 2.3	−42.68 ± 5.18	0.13 ± 0.01	124.54 ± 31.90
100 nm	PS-COOH	110 ± 6	−43.06 ± 0.82	0.03 ± 0.01	237.03 ± 26.44
200 nm	PS-COOH	200 ± 6	−44.54 ± 4.83	0.03 ± 0.03	206.57 ± 40.12
500 nm	PS-COOH	490 ± 75	−44.4 ± 1.19	0.13 ± 0.11	130.60 ± 79.47

[a] Polydispersity index. [b] Measured in the deionized H_2O, $n \geq 3$.

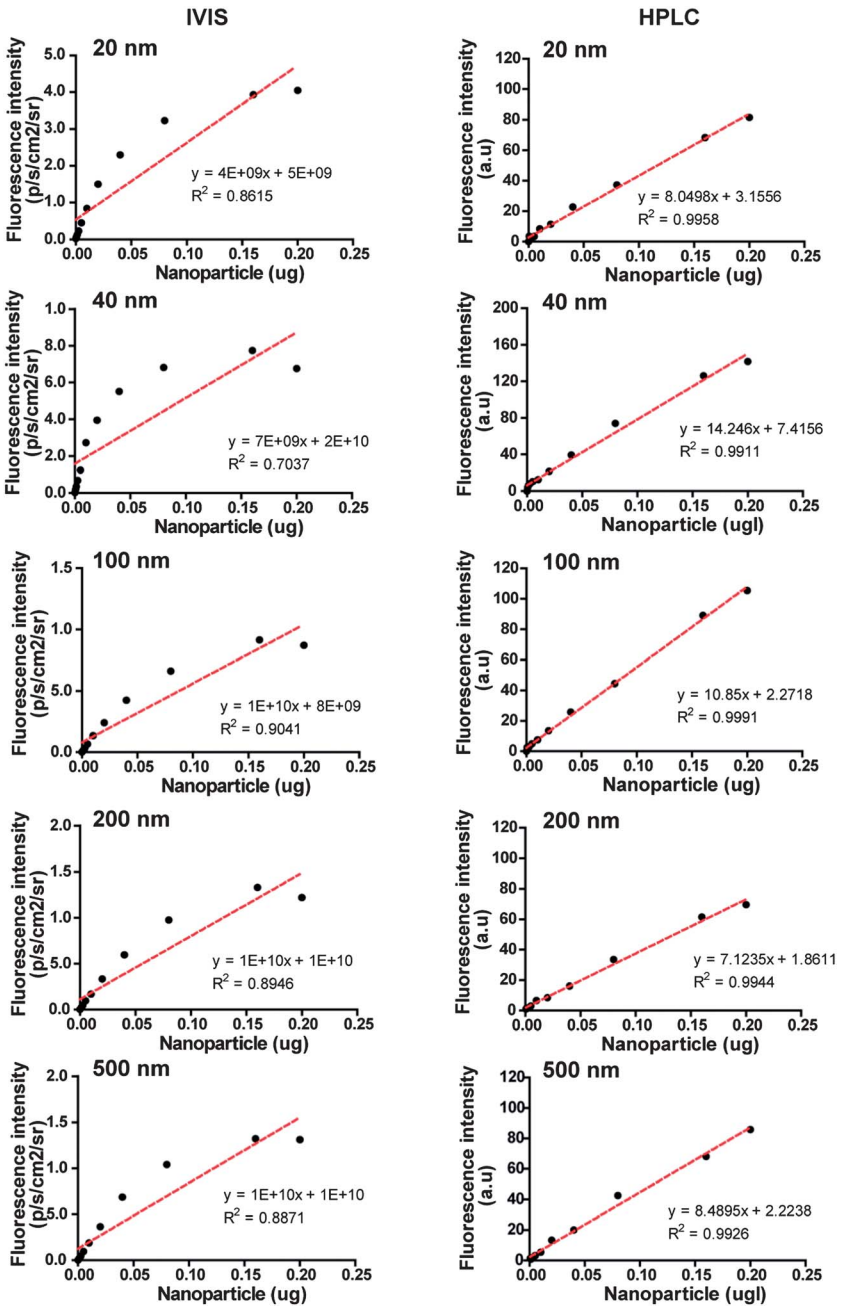

Fig. 1 Standard curve fittings from known concentrations of nanoparticle solutions analyzed by HPLC or IVIS.

compared to HPLC, indicating IVIS has a signal saturation problem when quantifying NPs. As a result, the increased linearity and sensitivity of HPLC is capable of providing comparatively more accurate results than IVIS.

Sample preparation for HPLC quantification of nanoparticles

NPs were injected into the jugular vein of mice to investigate their biodistribution (Fig. 2a). Of the most important benefits of using these NPs to study biodistribution is that the fluorescent signals are proportional to the amount of detected NPs (Fig. 2b). Furthermore, the NPs also showed dispersion stability and their sizes remained unchanged under various pH values (Fig. S2a†). However, it is important to note that the NPs displayed aggregation at pH 4 due to neutralization of the negative charge by hydrogen ions on the surface. Organs and tissues were first collected and digested in 1 M KOH overnight at 60 °C, and then mixed with *o*-xylene for dye extraction. Dye extraction was done by a liquid–liquid extraction before injection into the chromatograph. *o*-Xylene solvent is strong enough to dissolve the polystyrene NPs and then extracts the fluorescent dye within (Fig. S2b†). Dyes containing supernatants were analyzed with HPLC for NP quantity by measuring the fluorescence intensity. To ensure that the protocol did not compromise the NP fluorescence signal, stock NPs were treated with KOH and *o*-xylene at 60 °C overnight. HPLC analysis revealed an excellent alignment of the differently treated NP samples, indicating that neither KOH nor *o*-xylene interfered with the fluorescence signal (Fig. 2b). Standard calibration curves were also established by extracting different amounts of a NP stock solution with *o*-xylene before HPLC analysis (Fig. 1). Using detectors such as UV/VIS, fluorescence, refractive index, and mass-spectrometric (LC/MS), HPLC is a powerful tool to study the pharmacokinetics and biodistribution of NPs. HPLC purifies and quantifies specific molecules by taking advantage of different combinations of mobile and stationary phases. Studies by Oliveira *et al.* and Alhareth *et al.* also validated the use of HPLC in determining the pharmacokinetic and biodistribution of NPs.[16,27] In this study, however, we use different solvents to quantify the NPs inside the organs. Here, potassium hydroxide is used to digest tissues and then release NPs without fluorescein leakage. Notably, this leakage is the main concern when using HPLC for NP quantification as the solvent pairs used for extraction should not interfere with the NP signals.

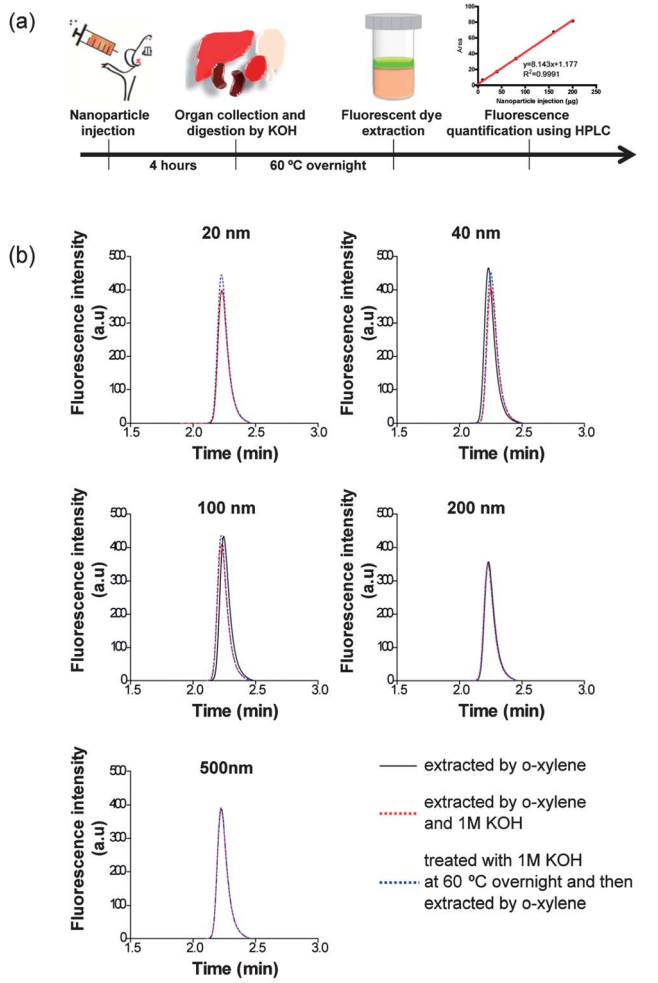

Fig. 2 Nanoparticle dye extraction and efficiency. (a) Flow chart of nanoparticle injection and dye extraction. (b) Fluorescence intensity of the dye extracted by different methods.

HPLC quantitative biodistribution profile in mice

NPs are well-known for their short half-lives within the blood circulation and their rapid accumulation (within hours) in target tissues or organs.[11] To verify this short-term biodistribution, 3 mg (comparable to the *in vitro* dose) of NPs were injected into the jugular vein of healthy FVB mice ($n \geq 6$) and allowed to circulate for 4 hours. Organs were collected separately for closer examinations on NP biodistribution. IVIS images revealed that NPs, regardless of size, were present in all of the vital organs, including the heart, lungs, liver, spleen, and kidneys (Fig. 3b). However, the fluorescence levels were extremely low in the brain when mice were injected with NPs larger than 100 nm. In contrast, HPLC revealed that the retention of larger sized NPs increased proportionally in the brain. HPLC seems to have detected an increased retention of larger NPs in the brain, but in fact, there was no actual difference (Fig. 3b). Retention of large NPs in the brain may be affected by the remaining fluorescein equivalents of NPs (Fig. S3a†). However, these NPs are present in such decimal quantity that it is difficult for HPLC detection. Thus, we must have enough NPs to analyze the brain tissue with HPLC. It is possible that the protection mechanism of the brain, the blood–brain-barrier, limits the access of these exogenous NPs to it. As a result, we induce systemic inflammation with LPS to sabotage the BBB permeability. We found under this condition, large sized NPs are significantly retained in the brain tissue (Fig. S4a†). HPLC quantification of the small sized NPs exhibit no observable difference under normal and LPS treated conditions (Fig. S4b†). Therefore, the amount of NPs influences HPLC quantification in the brain tissue. Moreover, IVIS and IHC cannot detect NPs beyond 100 nm, which is consistent with past studies. The whole field images demonstrate the distribution of 200 nm and

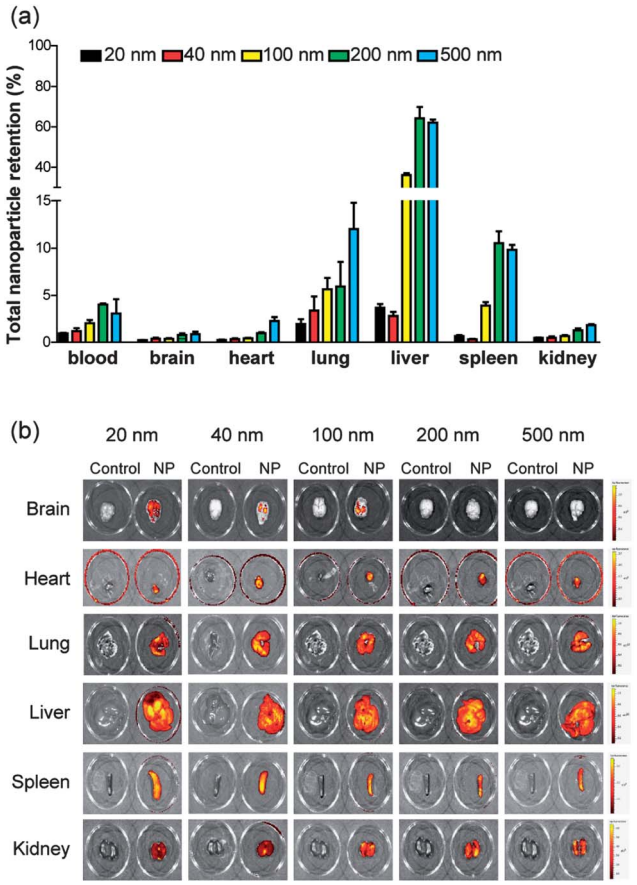

Fig. 3 The biodistribution of different-sized nanoparticles in normal mice. (a) Total nanoparticle retention in six vital organs and the blood by HPLC analysis. (b) IVIS images of the nanoparticle biodistribution in six vital organs.

500 nm NPs was closer to or on the outer surface of the brain cortex after LPS treatment which increased the permeability of vessels (Fig. S5 and 6†) and the ability to detect more signals when using IVIS (Fig. S4a†).

Although various techniques have been developed to study NP biodistribution,[21–23] many of them are still limited in their ability to detect trace amounts of NPs embedded in inner regions of the organs or tissues. For instance, IVIS cannot generate images accurately beyond a certain depth, which is dependent on the tissue and the fluorescence source.[20] HPLC quantification indicated that most of the NPs were retained in the lungs, liver, and spleen in a size-dependent manner (Fig. 3a) not shown in the IVIS results (Fig. 3b). For the liver, a steep cut-off size of 40 nm was determined. When we increased the NP size from 40 nm to 200 nm, NP retention in the liver increased from approximately 3% to more than 60%. Thus, we conclude that 200 nm is the optimal size for nano-carriers when targeting to the liver.

Biodistribution of the NPs analyzed by a weight-to-weight ratio of NPs to organs revealed a more even distribution of NP density among the heart, lungs, liver, spleen, and kidneys (Fig. S7†). The NPs retained in the heart and lungs are proportional to the NP size, suggesting that the larger NPs were blocked from exiting the capillaries to a greater extent. The spleen demonstrated a retention profile similar to the liver. NP density increased dramatically from 0.1 mg g^{-1} to more than 2.7 mg g^{-1} when the size increased from 40 nm to 200 nm. Again, this result suggests that 200 nm diameter may be the cut-off size when designing NPs to escape from the spleen.

Closer inspection of nanoparticle distribution in the tissue sections of the vital organs

To examine the NP distribution around the vessels at the tissue level, immunofluorescence staining was carried out in the vital organs. Consistent with HPLC results, larger NPs with sizes 200 and 500 nm located in the brain sections were not detectable using IVIS analysis (Fig. 4). All the differently sized NPs were detectable in all the vital organs, including the brain, lung, liver, spleen, heart, and kidney (Fig. 4 and S8†). More notably, all sizes of NPs were trapped in the isolectin-positive vessels. The biodistribution of these NPs was determined by size and blood flow, not NP extravasation. We noticed that larger NPs increased the chance of occlusion when compared to smaller NPs (Fig. 4, lung). Also, it appears that the NPs in the liver were evenly distributed over the entire tissue section. In contrast, those in the spleen were located mostly in the marginal zones. These tissue sections further confirmed the utilization of HPLC in NP biodistribution studies. Through immunohistochemical staining, whole field images demonstrate that most of the 200 nm and 500 nm NPs are located around the center of the brain. On the other hand, NPs smaller than 100 nm are retained primarily in the cerebral cortex and the white matter. However, quantification by IVIS analysis loses its accuracy when interpolating on the poor linear standard curves of all sizes of NPs. Thus, we used IVIS for preliminary surface biodistribution analysis, HPLC for precise biodistribution analysis and quantification and IHC for confirming NP location in the tissue.

Nanoparticle biodistribution in peripheral tissues

Most of the larger NPs (100 nm or greater) were retained in the vital organs and blood, but less than 20% of the smaller NPs (below 100 nm) were recovered from our samples (Fig. 5a). To assess the fate of the remainder of the smaller NPs, additional tissues and samples were analyzed, including samples of the skin, muscle, adipose tissue (fat), and urine. HPLC quantification confirmed that the retention of NPs in the peripheral tissues was inversely proportional to the size of the NPs (Fig. 5b). Therefore, NPs distribute differently among organs and are excreted according to size. Larger NPs are more likely to be retained in the vital organs. Smaller NPs have the ability to permeate more easily throughout the vasculature, pass through the renal system into the urine, and distribute into the peripheral tissues. Components within the renal system, such as the glomerular endothelium or the glomerular basal membrane, filter small substances through a size-specific pore.[24] As such, most NPs within the kidneys were found to accumulate in the glomerulus (Fig. S8,† kidney). Together with the finding that smaller NPs were 2 to 3 times more likely to be found in the urine, the glomerulus was confirmed as a filter for 100 nm particles (Fig. 5b).

This study systematically characterizes the size-dependent biodistribution of NPs ranging from 20 to 500 nm in mice.

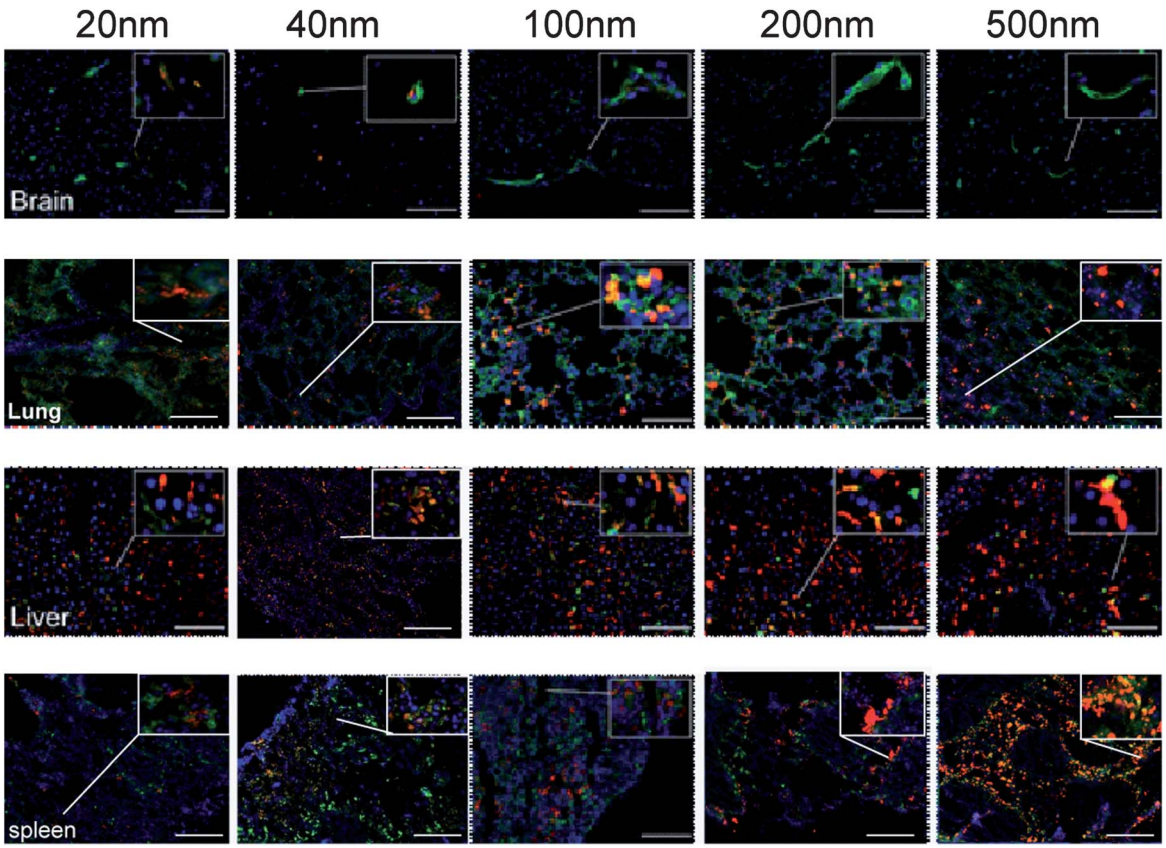

Fig. 4 The tissue retention of nanoparticles of different sizes in the major vital organs of mice. Immunofluorescent staining of tissue sections showing a size effect of nanoparticle retention in the brain, lungs, liver, and spleen in normal mice. Red, nanoparticles; green, isolectin; blue, DAPI. Scale bar: 100 μm.

Analysis through HPLC demonstrates that most of the vital organs retain NPs in a size-dependent manner. One should be cautious when examining the biodistribution of NPs with fluorescence imaging system such as IVIS. Previous report has shown that optically inhomogeneous samples may influence detection from a light source and consequently alter quantification of NPs.[17] We performed half-fold dilutions of the same mass NPs to obtain approximately 10 concentrations and examined their fluorescence intensity *via* HPLC and IVIS. The HPLC method was sensitive to much lower dilutions and could generate a signal compared to the IVIS method. We found an 8-fold difference by dividing the minimal detectable concentrations of HPLC and IVIS. Also, the R^2 value of HPLC standard curve is significantly greater than that of IVIS. Therefore, HPLC is more suitable for analyzing NP biodistribution. Under normal conditions, nanoparticles larger than 100 nm are more likely to be retained in the vital organs. In contrast, NPs smaller than 100 nm are mostly distributed in the peripheral tissues or excreted *via* urine. We believe that size is the largest contributor to NP distribution. However, due to the limitations of the study, the weight and number of NPs in each treatment group cannot be maintained the same concurrently. We chose to maintain the same weight in our experimental set-up, similar to past studies.[25,26]

A better understanding of the size-dependency of NPs will lay the foundation to develop and achieve more effective diagnostics and therapies for clinical use. Several concerns, particularly the time dependent effects, must be taken into consideration when studying nanomedicine biodistribution and therapeutic NP designs. Conventionally, biodistribution is examined at only one time point. Choi *et al.* demonstrated a size-dependent manner of NP distribution in mice after 24 hours of circulation in which NP retention in the kidney was found to be inversely proportional to NP size.[9] Interestingly, our results show the opposite where larger-sized NPs are more retained than smaller ones in the kidney. We suspect that NP clearance may be the reason for discrepancy between NP retention at 4 and 24 hours in the kidney. HPLC data also reveal that the majority of the large sized NPs are retained in the vital organs 4 hours after injection whereas smaller sized NPs are only retained in the peripheral tissues. Taken together, there is a limited time window for drug delivery and thus, identification of this window is critical for optimizing therapeutic efficiency. In help of future nanomedicine applications, we rely on a precise quantification method and HPLC fulfills this need. Even though HPLC cannot provide information in long time periods compared to IVIS, the combination of these systems complement one another.

Conclusions

In conclusion, the study has both systemically and quantitatively characterized the biodistribution of different sized NPs in

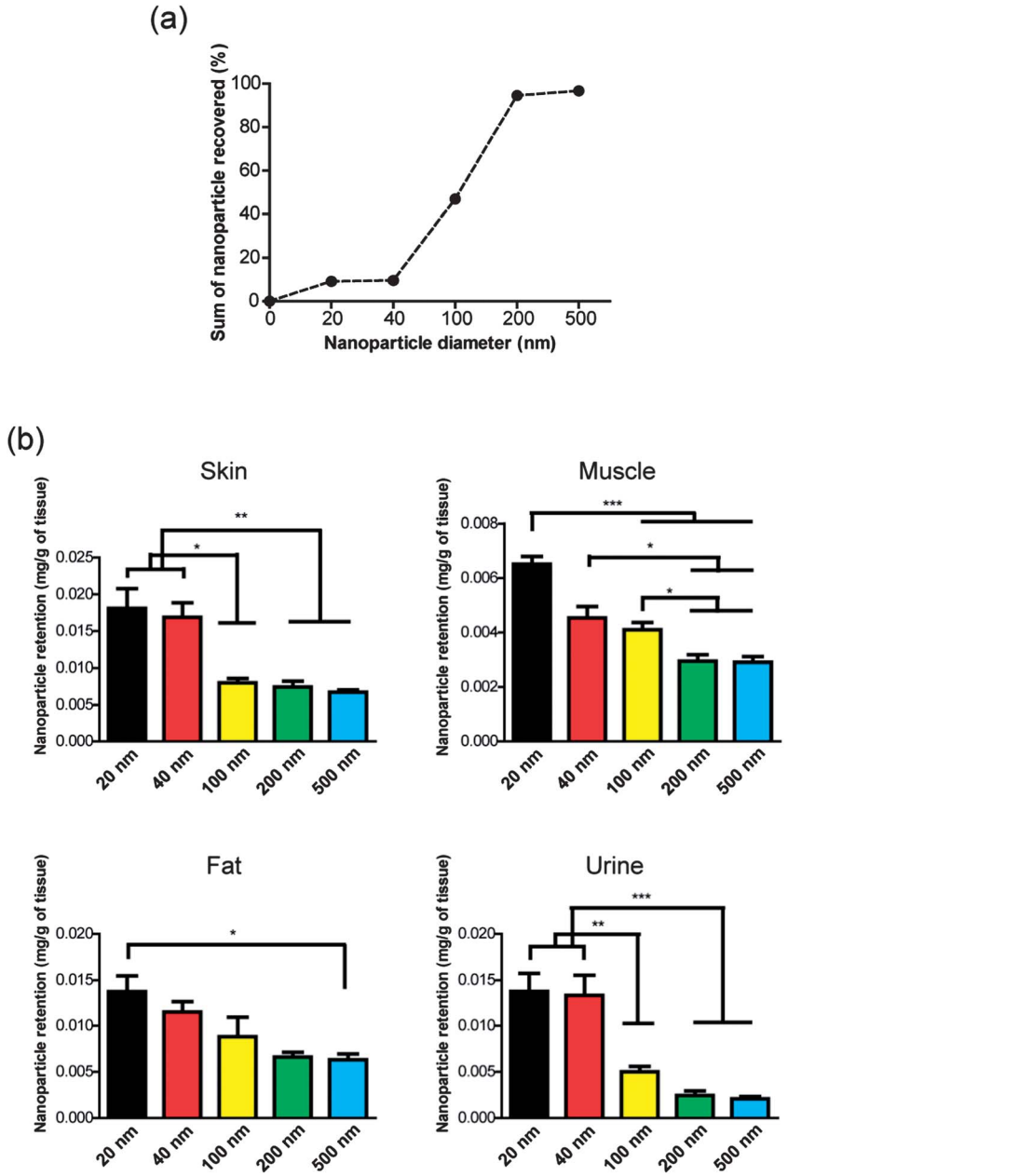

Fig. 5 The size effect of nanoparticle retention in the vital or peripheral organ and tissues. (a) The sum of the total nanoparticle retention in the six vital organs by nanoparticle size. (b) Nanoparticle retention in peripheral tissues and urine quantified by HPLC. *$p < 0.05$; **$p < 0.01$; ***$p < 0.001$.

mice. This biodistribution of NPs is size-dependent. These results provide essential characterizations that will be useful in nanomedicine design. The conclusions drawn from this study should be taken into account when designing intravenously delivered drugs, whether to increase the drug efficacy or to reduce the side effects.

Acknowledgements

We thank the Department of Chemistry of NCKU for TEM imaging assistance and the Tissue Bank Core Facility at the NCKU Hospital for tissue section preparations. We also thank M. O'Donnell (University of Washington), P. J. Lu (NCKU), S. R. Roffler (Academia Sinica) and H. W. Li (National Taiwan University) for discussion. This work was supported by the National Science Council grants 100-2314-B-006-046, 101-2325-B-006-013 and 99-2628-B-006-029; the National Health Research Institutes grant EX102-10123SI and EX102-10026SI; the National Research Program for Biopharmaceuticals grants DOH102-TD-PB-111TM019 and DOH102-TD-PB-111-TM020; and the Academia Sinica Translational Medicine Program. Our appreciation is extended to NCKU TissueBank for frozen sections, Mr H. T. Lin of Regional Instruments Center at NSYSU for his help on TEM experiments.

Notes and references

1 D. G. Anderson, J. A. Burdick and R. Langer, *Science*, 2004, **305**, 1923–1924.
2 R. Langer and D. A. Tirrell, *Nature*, 2004, **428**, 487–492.
3 S. Sengupta, D. Eavarone, I. Capila, G. Zhao, N. Watson, T. Kiziltepe and R. Sasisekharan, *Nature*, 2005, **436**, 568–572.
4 K. A. Woodrow, Y. Cu, C. J. Booth, J. K. Saucier-Sawyer, M. J. Wood and W. M. Saltzman, *Nat. Mater.*, 2009, **8**, 526–533.
5 A. Ito, E. Hibino, C. Kobayashi, H. Terasaki, H. Kagami, M. Ueda, T. Kobayashi and H. Honda, *Tissue Eng.*, 2005, **11**, 489–496.
6 S. Sarkar, G. Y. Lee, J. Y. Wong and T. A. Desai, *Biomaterials*, 2006, **27**, 4775–4782.
7 H. S. Choi, W. Liu, P. Misra, E. Tanaka, J. P. Zimmer, B. I. Ipe, M. G. Bawendi and J. V. Frangioni, *Nat. Biotechnol.*, 2007, **25**, 1165–1170.
8 S. Lee, E. J. Cha, K. Park, S. Y. Lee, J. K. Hong, I. C. Sun, S. Y. Kim, K. Choi, I. C. Kwon, K. Kim and C. H. Ahn, *Angew. Chem., Int. Ed.*, 2008, **47**, 2804–2807.
9 C. H. Choi, J. E. Zuckerman, P. Webster and M. E. Davis, *Proc. Natl. Acad. Sci. U. S. A.*, 2011, **108**, 6656–6661.
10 H. S. Choi, W. Liu, F. Liu, K. Nasr, P. Misra, M. G. Bawendi and J. V. Frangioni, *Nat. Nanotechnol.*, 2010, **5**, 42–47.
11 S. D. Li and L. Huang, *Mol. Pharmaceutics*, 2008, **5**, 496–504.
12 D. S. Kohane, *Biotechnol. Bioeng.*, 2007, **96**, 203–209.
13 M. G. Kong, M. Keidar and K. Ostrikov, *J. Phys. D: Appl. Phys.*, 2011, **44**, 1–14.
14 M. Caldorera-Moore, N. Guimard, L. Shi and K. Roy, *Expert Opin. Drug Delivery*, 2010, **7**, 479–495.
15 A. E. Nel, L. Madler, D. Velegol, T. Xia, E. M. Hoek, P. Somasundaran, F. Klaessig, V. Castranova and M. Thompson, *Nat. Mater.*, 2009, **8**, 543–557.
16 L. T. Oliveira, G. M. Garcia, E. K. Kano, A. C. Tedesco and V. C. Mosqueira, *J. Pharm. Biomed. Anal.*, 2011, **56**, 70–77.
17 Y. Liu, Y. C. Tseng and L. Huang, *Pharm. Res.*, 2012, **29**, 3273–3277.
18 G. J. Mahler, M. B. Esch, E. Tako, T. L. Southard, S. D. Archer, R. P. Glahn and M. L. Shuler, *Nat. Nanotechnol.*, 2012, **7**, 264–271.
19 M. L. Springer, T. K. Ip and H. M. Blau, *Mol. Ther.*, 2000, **1**, 82–87.
20 S. Keren, O. Gheysens, C. S. Levin and S. S. Gambhir, *IEEE Trans. Med. Imaging*, 2008, **27**, 58–63.
21 D. W. Bartlett, H. Su, I. J. Hildebrandt, W. A. Weber and M. E. Davis, *Proc. Natl. Acad. Sci. U. S. A.*, 2007, **104**, 15549–15554.
22 M. J. E. Lee, O. Veiseh, N. Bhattarai, C. Sun, S. J. Hansen, S. Ditzler, S. Knoblaugh, D. Lee, R. Ellenbogen, M. Q. Zhang and J. M. Olson, *PLoS One*, 2010, **5**, 1–8.
23 M. Nahrendorf, H. W. Zhang, S. Hembrador, P. Panizzi, D. E. Sosnovik, E. Aikawa, P. Libby, F. K. Swirski and R. Weissleder, *Circulation*, 2008, **117**, 379–387.
24 F. C. Luft, G. R. Aronoff, A. P. Evan, B. A. Connors, D. K. Blase and V. H. Gattone, *Antimicrob. Agents Chemother.*, 1982, **21**, 830–835.
25 D. P. Lankveld, A. G. Oomen, P. Krystek, A. Neigh, A. Troost-de Jong, C. W. Noorlander, J. C. Van Eijkeren, R. E. Geertsma and W. H. De Jong, *Biomaterials*, 2010, **31**, 8350–8361.
26 S. K. Balasubramanian, K. W. Poh, C. N. Ong, W. G. Kreyling, W. Y. Ong and L. E. Yu, *Biomaterials*, 2013, **34**, 5439–5452.
27 K. Alhareth, C. Vauthier, C. Gueutin, G. Ponchel and F. Moussa, *J. Chromatogr. B: Anal. Technol. Biomed. Life Sci.*, 2012, **887**, 128–132.

